PCCP

PAPER

View Article Online
View Journal | View Issue

Cite this: *Phys. Chem. Chem. Phys.*, 2016, **18**, 15774

Chemical bonding and dynamic fluxionality of a B_{15}^+ cluster: a nanoscale double-axle tank tread†

Ying-Jin Wang,[ab] Xue-Rui You,[a] Qiang Chen,[ab] Lin-Yan Feng,[a] Kang Wang,[a] Ting Ou,[a] Xiao-Yun Zhao,[a] Hua-Jin Zhai*[ac] and Si-Dian Li*[a]

Received 16th April 2016,
Accepted 16th May 2016

DOI: 10.1039/c6cp02544g

www.rsc.org/pccp

A planar, elongated B_{15}^+ cationic cluster is shown to be structurally fluxional and functions as a nanoscale tank tread on the basis of electronic structure calculations, bonding analyses, and molecular dynamics simulations. The outer B_{11} peripheral ring behaves like a flexible chain gliding around an inner B_4 rhombus core, almost freely at the temperature of 500 K. The rotational energy barrier is only 1.37 kcal mol^{-1} (0.06 eV) at the PBE0/6-311+G* level, further refined to 1.66 kcal mol^{-1} (0.07 eV) at the single-point CCSD(T)/6-311G*//CCSD/6-311G* level. Two soft vibrational modes of 166.3 and 258.3 cm^{-1} are associated with the rotation, serving as double engines for the system. Bonding analysis suggests that the "island" electron clouds, both σ and π, between the peripheral ring and inner core flow and shift continuously during the intramolecular rotation, facilitating the dynamic fluxionality of the system with a small rotational barrier. The B_{15}^+ cluster, roughly 0.6 nm in dimension, is the first double-axle nanoscale tank tread equipped with two engines, which expands the concepts of molecular wheels, Wankel motors, and molecular tanks.

1. Introduction

The fascinating performance of nanomachines has inspired considerable interest in the design and fabrication of nanovehicles, such as nanocars, nanotrucks, wheelbarrows, and nanowalkers.[1,2] Owing to its intrinsic electron-deficiency, boron is a suitable candidate for novel low-dimensional nanostructures. During the past decade, a series of experiments and quantum chemical calculations have shown that elemental boron clusters favor unique planar or quasi-planar structures over a wide range of sizes: B_n^- (n = 3–25, 27, 30, 35, 36, 40) for anionic boron clusters,[3–16] B_n (n up to at least 20) for neutral clusters,[16] and B_n^+ (n up to 16) for cationic clusters.[17] The flat world of boron clusters is governed by the localized two-center two-electron (2c-2e) σ bonds on the periphery *versus* the delocalized multicenter bonds (nc-2e) in both σ and π frameworks,[3–8] the latter rendering (σ and π) aromaticity, antiaromaticity, or conflicting aromaticity to the systems. Planar or quasi-planar boron clusters offer opportunities to design intriguing free-standing boron nanostructures, such as planar hypercoordinate molecular wheels (B_8^{2-} and B_9^-),[3] concentric dual π aromatic clusters,[9] and molecular disks.[10]

The electron-deficiency of boron can further lead to structural fluxionality for certain boron-based nanosystems, allowing the discovery of interesting molecular dynamics (MD) properties. Indeed, molecular Wankel motors (B_{19}^-, B_{13}^+, and B_{18}^{2-})[18–20] and nanoscale tank treads (B_{11}^- and B_{11})[21] were reported lately. The Wankel motors are built upon an idea from the model boron–carbon clusters,[22] which were known not to be the global-minimum (GM) structures on their potential energy surfaces.

The MD properties of planar, elongated boron clusters have not been explored until very recently, when the present authors demonstrated computationally that the planar, elongated B_{11}^- and B_{11} clusters behave like moving nanoscale "tank treads" at room temperature.[21] In contrast to molecular wheels[3] or Wankel motors,[18–20] which possess a rigid, circular outer ring, the B_{11}^- and B_{11} clusters consist of a prolate, flexible B_9 peripheral ring, gliding around an elongated B_2 core. This MD behavior is beyond imagination, because the elongated B_2 core may be intuitively considered by many as a "bar" that halts such intramolecular motion. In this work, we show that the B_{11}^- and B_{11} clusters are not isolated examples of nanoscale tank treads. We examine the structure, chemical bonding, and MD properties of the cationic B_{15}^+ cluster, which consists of an elongated, diamond-shaped or rhombic B_4 core and a prolate B_{11} peripheral ring. The B_{15}^+ cluster was first characterized experimentally in

[a] *Nanocluster Laboratory, Institute of Molecular Science, Shanxi University, Taiyuan 030006, China. E-mail: hj.zhai@sxu.edu.cn, lisidian@sxu.edu.cn*
[b] *Department of Chemistry, Xinzhou Teachers University, Xinzhou 034000, China*
[c] *State Key Laboratory of Quantum Optics and Quantum Optics Devices, Shanxi University, Taiyuan 030006, China*

† Electronic supplementary information (ESI) available: A short movie of the Born–Oppenheimer molecular dynamics simulations of B_{15}^+ at 500 K; canonical molecular orbitals (CMOs) of the global-minimum (GM) and transition state (TS) structures of B_{15}^+; the bonding pattern of the TS structure of B_{15}^+ *via* the electron localization functions (ELFs) and adaptive natural density partitioning (AdNDP) analyses; the evolution of ELF_σ against the bifurcation value for the C_{2v} global minimum of B_{15}^+; and the Cartesian coordinates for B_{15}^+ C_{2v} ($^1A_1$) GM and its TS at the PBE0/6-311+G* level. See DOI: 10.1039/c6cp02544g

2007 using the ion mobility technique[17] and it is therefore a real molecule. It has a rough size of 0.6 nm in width and 0.5 nm in height. Our computational data indicate that the B_{15}^+ cluster is structurally fluxional as a nanoscale tank tread at 500 K. The rotational barrier is only 1.66 kcal mol^{-1} (0.07 eV) at the CCSD(T)/6-311G*//CCSD/6-311G* level. Interestingly and remarkably, it is not just a slight increase in size from B_{11}^- and B_{11} clusters to the B_{15}^+ cluster, the latter has new chemical and dynamical insights to offer. We propose a bonding model for B_{15}^+, whose delocalized bonding includes 10σ electrons for the interaction between the peripheral B_{11} ring and the rhombic B_4 core, 4σ electrons primarily for the rhombic B_4 core, and 8π electrons that are globally delocalized. Thus the B_{15}^+ cluster possesses global σ aromaticity and π antiaromaticity, as well as σ antiaromaticity for the B_4 core. The π framework of B_{15}^+ is proposed to be analogous to that in the hydrocarbon molecules: C_{2v} C_7H_7 and D_{2d} C_8H_8. The present bonding model for B_{15}^+ helps elucidate the unique MD behaviors of the system. In particular, we show that the B_{15}^+ cluster possesses two rotational centers, in contrast to only one in B_{11}^- and B_{11} clusters.[21] The intramolecular rotation of B_{15}^+ proceeds around two axles, which appears to be driven by two soft vibrational modes, or dubbed "double engines". The concept of double engines may be extended to multiple engines, which should drive the motion of more sophisticated, elongated nanosystems. To date, such nanosystems have remained unknown in the literature.

2. Computational methods

The GM structure of B_{15}^+ (C_{2v}, $^1A_1$) was constructed based on the literature[4,5,17] and fully reoptimized at the PBE0/6-311+G*[23,24] and CCSD/6-311G* levels using the Gaussian 09 package,[25] including vibrational frequency calculations. The QST2 calculation was performed to search the transition state (TS) for the intramolecular rotation, which turned out to have C_{2v} symmetry as well. Intrinsic reaction coordinate (IRC) calculations were carried out to confirm that the TS structure is truly associated with the GM. To evaluate the rotational barrier accurately, further calculations were carried out at the single-point CCSD(T)/6-311G*//CCSD/6-311G* level.[26]

Born–Oppenheimer molecular dynamics (BOMD) simulations were performed at the PBE level using the CP2K software package,[27] at the temperatures of 300, 500, and 900 K. Bonding analyses were performed using the canonical molecular orbitals (CMOs), electron localization functions (ELF),[28] and adaptive natural density partitioning (AdNDP); the latter being developed by Zubarev and Boldyrev.[29] Since the AdNDP method is not sensitive to the level of theory or the basis set used, we chose the PBE0/6-31G level for the AdNDP calculations. The visualization of the ELF and AdNDP results were realized using the Molekel 5.4.0.8 program.[30]

3. Results and discussion

3.1. The vibrational frequencies and molecular dynamics

The 2007 computational results of Oger *et al.*[17] suggest that the GM of the B_{15}^+ cluster consists of a rhombic B_4 core enclosed by a peripheral B_{11} ring with C_s symmetry. We have constructed herein the C_s B_{15}^+ cluster according to ref. 17, which serves as the initial structure in our PBE0/6-311+G* calculations. However, upon structural optimization at PBE0, the GM structure of B_{15}^+ does not adopt C_s symmetry; rather it has a higher symmetry of C_{2v}. Since the PBE0 method has been extensively utilized and tested in recent studies on boron clusters,[13–15] we believe that the C_{2v} structure is the true GM for B_{15}^+. To further confirm this, we have run full structural optimizations and frequency calculations for B_{15}^+ at the CCSD/6-311G* level and found that it indeed possesses the C_{2v} GM structure. Note that the current C_{2v} GM structure is similar to the C_s structure in ref. 17 in overall shape, and thus the former should not differ much from the latter in terms of collision cross sections in ion mobility experiments. Therefore, the present C_{2v} GM structure of B_{15}^+ may account for the ion mobility data as well.

The C_{2v} GM structure of B_{15}^+ at the PBE0/6-311+G* level is depicted in Fig. 1(a), along with the bond distances. The C_{2v} GM of B_{15}^+ has a horizontal C_2 axis along the B1–B12–B14 direction, around which four rhombic B_4 holes are located symmetrically: B11B10B15B12 and B8B9B15B14 on the top *versus* B2B3B13B12 and B5B4B13B14 at the bottom. These rhombic holes are the most flexible parts in the GM structure, which provide the structural basis for dynamic fluxionality in the cluster.

Vibrational frequency analyses indicate that the B_{15}^+ cluster possesses a soft mode of 166.3 cm^{-1} at PBE0/6-311+G* (Fig. 2(a)), which corresponds to the in-plane rotation of the peripheral B_{11} ring with respect to the B_4 core. Following this mode, a TS structure is located straightforwardly; see Fig. 1(b). The TS structure also has C_{2v} symmetry with one imaginary frequency of 115.7i cm^{-1} (Fig. 2(b)). This imaginary frequency is also related to the intramolecular rotation of B_{15}^+. More interestingly, besides the small vibrational frequency, there exists another slightly higher vibrational mode of 258.3 cm^{-1} in the GM

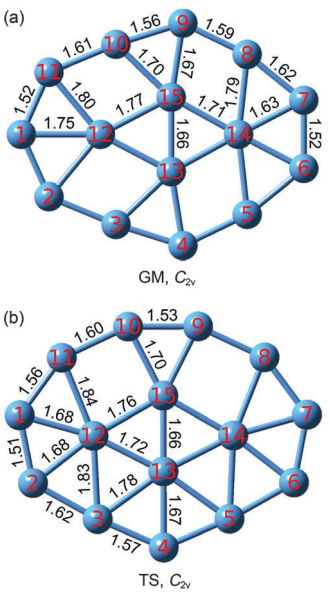

Fig. 1 Optimized structures of (a) the C_{2v} ($^1A_1$) global minimum (GM) and (b) the C_{2v} ($^1A_1$) transition state (TS) of B_{15}^+ at the PBE0/6-311+G* level. Bond distances are indicated in Å.

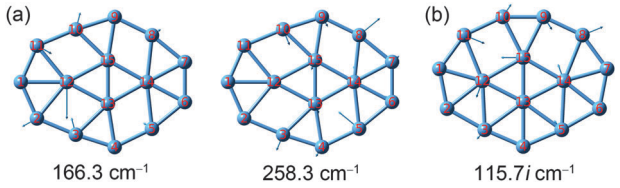

Fig. 2 The displacement vectors of the soft vibrational modes relevant to the intramolecular rotation of B_{15}^+. (a) Global minimum. (b) Transition state.

structure (Fig. 2(a)), which also corresponds to the intramolecular rotation.

The soft mode of 166.3 cm^{-1} for the GM structure of B_{15}^+ and its corresponding imaginary frequency of 115.7i cm^{-1} for the TS represent a pair of vibrational modes, the former primarily driving the rhombus-to-square transformation of the four-membered B11B10B15B12 and B2B3B13B12 holes (Fig. 1(a)). This mode involves notably the B10B12 and B3B12 stretches (Fig. 2(a)). In the MD process, the mode may start the motion with a stretch of the B10B12 distance, which turns the B11B10B15B12 rhombus to a square. During this motion, the B15B8 distance expands accordingly (albeit to a less extent), and the B8B9B15B14 rhombus is transformed to a square as well. These two squares are precisely, symmetrically located around the C_2 axis of the TS structure (Fig. 1(b)), which is now vertically oriented, that is, with a 90° in-plane rotation relative to the C_2 axis in the GM. The stretches of B10B12 and B15B8 move the B11/B10/B9/B8 atoms clockwise around the B_4 core. In the meantime, this soft mode generates a shrink of the B3B12 distance in the GM, making the B2B3B13B12 rhombus more acute in shape. The movement in turn also pushes the B13B5 distance closer, making the B5B4B13B14 rhombus more acute. The shrinks of B3B12 and B13B5 facilitate the clockwise rotation of the B2/B3/B4/B5 atoms, and probably the B6 atom.

Thus, initiated by the stretching of B10B12 and the shrinking of B3B12, the 166.3 cm^{-1} mode manages to push/pull the majority of B atoms in the peripheral ring clockwise. For the next period of the vibration, the B10B12 distance shrinks and that of B3B12 expands, leading to the counter-clockwise in-plane rotation of the peripheral B_{11} ring with respect to the B_4 core. In short, the soft mode can be considered as an engine that drives the intramolecular rotation of the B_{15}^+ cluster, which can be either clockwise or counter-clockwise. Such rotation is rather similar to that of the recently reported B_{11}^- and B_{11} clusters.[21] An additional vibrational mode in the GM of B_{15}^+, 258.3 cm^{-1} (Fig. 2(a)), may also contribute to the intramolecular rotation, which will be discussed below in Section 3.5.

For the TS structure of B_{15}^+, the imaginary frequency of 115.7i cm^{-1} (Fig. 2(b)) corresponds to the reversed square-to-rhombus transformation of the B11B10B15B12 and B8B9B15B14 holes. This is driven by a horizontal movement of the B15 atom. When B15 moves toward the right, the B11B15 distance expands and that of B10B12 shrinks. As a consequence, the TS structure turns back to the initial GM structure. On the other hand, the movement of B15 toward the left gives rise to another, equivalent C_{2v} GM, whose C_2 axis is rotated by 180° with respect to the initial GM.

The rotational energy barrier for B_{15}^+ is evaluated to be 1.37 kcal mol^{-1} at the PBE0/6-311+G* level, with zero-point energy (ZPE) corrections. The barrier is further refined to 1.66 kcal mol^{-1} at the single-point CCSD(T)/6-311G*//CCSD/6-311G* level, which is minor in particular considering the elongated overall shape of B_{15}^+. In contrast to the circular shapes of the molecular wheels (B_8^{2-} and B_9^-)[3] and Wankel motors (B_{19}^-, B_{13}^+, and B_{18}^{2-}),[18–20] the B_{15}^+ GM has a width of 6.26 Å *versus* a height of 4.95 Å, and those of the TS are 6.29 *versus* 4.84 Å. These values indicate a height-to-width ratio of 4 : 5, suggesting that B_{15}^+ is a relatively prolate cluster and the intramolecular rotation of the outer chain around the rhombic B_4 core is generally not anticipated. Such a small barrier hints the likelihood of almost free intramolecular rotation for the B_{15}^+ cluster.

To demonstrate the structural fluxionality of B_{15}^+, the BOMD simulations were performed at the PBE/DZVP-GTH level, starting from the equilibrium GM geometry with random velocities assigned to the atoms. The system was equilibrated at 300, 500, and 900 K, respectively, using a Nosé–Hoover thermal bath for 20 ps, after which a set of 40 ps trajectories were computed. It is routine to perform BOMD calculations at a lower level of theory than that for cluster structural calculations, because the former are too computationally demanding at a higher level. We note that the PBE/DZVP-GTH level of theory gives an energy barrier of 1.22 kcal mol^{-1} (0.05 eV) for this system, which is remarkably close to that at the PBE0/6-311+G* level (1.37 kcal mol^{-1}, or 0.06 eV). The BOMD calculations positively confirm the fluxionality of B_{15}^+. During the simulations, the B_{15}^+ cluster maintains basically its planar, elongated geometry, and the peripheral atoms rotate almost freely around the rhombic B_4 core.

Note that the rotation at 300 K appears to be somewhat difficult for B_{15}^+, which is reasonable in view of the slightly higher rotational barrier than those of previously reported boron Wankel motors or tank treads.[18–21] Nonetheless, at 500 K the B_{15}^+ cluster functions dynamically as a moving tank tread, that is, the peripheral B_{11} ring glides like a flexible chain around the rhombic B_4 core. An extracted short movie illustrating the intramolecular rotation of B_{15}^+ at 500 K is provided in the ESI,† which covers a time span of about 30 ps. At a high temperature of 900 K, B_{15}^+ also appears to be robust and functions as usual.

3.2. A proposed chemical bonding model with three-fold electron delocalization

The key to the fluxional behaviors of the B_{15}^+ cluster lies in its bonding. Certain aspects of the bonding were discussed in the literature for B_{15}^- and B_{15} clusters, but not the B_{15}^+ cluster. Zhai *et al.*[4] first reported the GM structures of B_{15}^- and B_{15} and found that B_{15}^- is an aromatic system with 10π electrons, conforming to the (4*n* + 2) Hückel rule. Boldyrev and coworkers[5] subsequently suggested a plausible bonding model[8] for B_{15}^- on the basis of natural bond orbital (NBO) analysis. The model consists of eleven 2c-2e σ bonds for the outer ring, four "assumed" 2c-2e σ bonds for the B_4 core, four globally delocalized π bonds, and four globally delocalized σ bonds, where the last two subsets of bonds were claimed to render (π and σ) double antiaromaticity

for B_{15}^-. It is stressed that the Boldyrev model[8] for B_{15}^- is tentative, rather than conclusive.

We propose herein that the B_{15}^+ cluster, an elongated system consisting of a rhombic B_4 core and a peripheral B_{11} ring, may be faithfully viewed from an alternative perspective as the combination of four structural blocks: two triangular B_3 (B9B10B15 and B3B4B13), one rhombic B_4 (B1B2B12B11), and one trapezoid B_5 (B5B6B7B8B14) (Fig. 1(a)). The structural blocks fuse together *via* two links between each two adjacent units, where the four inner links form a rhombic B_4 core and the four outer links become a portion of the peripheral B_{11} ring. Indeed, B_n (n = 3–5) clusters were established recently to be key structural blocks in low-dimensional boron nanostructures.[31,32]

The B_{15}^+ cluster is an electronic system with 44 valence electrons, which occupy 22 CMOs as depicted in Fig. 3 and the ESI† (Fig. S1). While every CMO in B_{15}^+ appears to be delocalized, the 22 CMOs can be sorted to four subsets[33] according to the type of atomic orbitals (AOs): (i) 11 CMOs for the s/p_t σ framework (Fig. S1, ESI†), where "t" represents the tangential component with respect to the outer B_{11} and inner B_4 rings; (ii) 5 CMOs for the radial p_r σ framework (Fig. 3(a)); (iii) 4 CMOs for the perpendicular p_π framework (Fig. 3(c)); and (iv) the remaining two CMOs associated with the σ bonding in the inner B_4 core (Fig. 3(b)). Notably, the tangential s/p_t σ, radial p_r σ, and p_π CMOs show one-to-one correspondence with each other from the bottom-up in terms of the overall spatial distribution of electron clouds, suggesting that subsets (i)–(iii) are equally critical for the bonding of the system, except that they differ in the number of occupied electrons. Thus the three subsets should be treated independently. Of these, Boldyrev *et al.*[8] correctly assigned the p_π framework in B_{15}^- with 4 CMOs for antiaromaticity, as well as its s/p_t σ framework with 11 CMOs. However, the nature of the radial p_r σ framework and the bonding in the inner B_4 core have remained unclear.[3,8] We shall provide here an updated, complete bonding model for the B_{15}^+ cluster, which is also applicable to the B_{15}^- and B_{15} clusters.

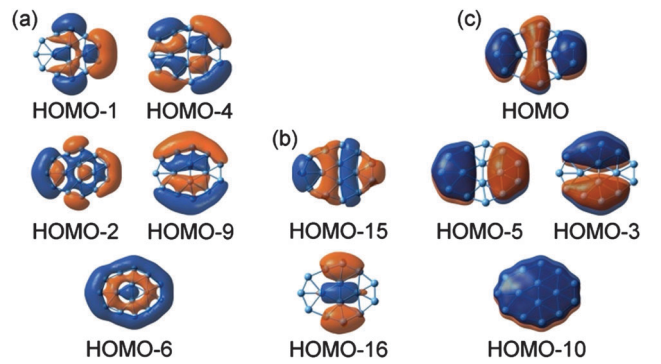

Fig. 3 Selected canonical molecular orbitals (CMOs) of the C_{2v} ($^1A_1$) global minimum of the B_{15}^+ cluster. (a) Five delocalized σ bonds. (b) Two delocalized σ bonds associated with the inner rhombic B_4 core. (c) Four delocalized π bonds. The delocalized π and σ bonds, (c) *versus* (a), show one-to-one correspondence with each other. The 10σ and 8π electrons, respectively, conform to the $(4n + 2)/4n$ Hückel rules for aromaticity/antiaromaticity. The inner B_4 rhombus with 4σ electrons is considered to be σ antiaromatic.

The CMOs for B_{15}^+ in the above subset (i) are readily localized to eleven 2c-2e σ bonds along the peripheral B_{11} ring. However, the CMOs in subsets (ii) through (iv) cannot be transformed to localized 2c-2e B–B bonds. Similar to B_{15}^-,[8] the B_{15}^+ cluster has 4 globally delocalized π CMOs, that is, subset (iii), whose 8π counting conforms to the $4n$ Hückel rule, rendering π antiaromaticity for B_{15}^+. The 5 radial p_r σ CMOs of B_{15}^+, that is, subset (ii), are closely analogous to the p_π CMOs in terms of the overall pattern and electron cloud distributions, except for the difference in the nature of p_π *versus* radial p_r σ. The p_r σ framework should thus also be globally delocalized, whose 10σ electrons render σ_r aromaticity for B_{15}^+.

Despite the mixture from the outer ring, the two CMOs in subset (iv) contain a major component for σ bonding in the inner B_4 core. HOMO−16 is completely bonding between the four B centers. HOMO−15 is partially bonding/antibonding: bonding between B13 and B15 (shorter diagonal for the rhombic core) *versus* antibonding between B12 and B14 (longer diagonal). The combination of HOMO−16/HOMO−15 is rather similar to that in the rhombic Li_4 cluster (Fig. 4(a) *versus* Fig. 4(b)), a prototypical σ antiaromatic system,[34] indicating that the rhombic B_4 core in the B_{15}^+ cluster should possess σ antiaromaticity as well. Note that the square-to-rhombus distortion is a characteristic structural consequence of σ antiaromaticity for a tetraatomic system, analogous to the square-to-rectangle structural distortion for π antiaromaticity. Interestingly, Boldyrev and coworkers[8] found in their NBO analysis a number of "lone-pairs" with occupation numbers (ONs) of about 1.1 for the central B atoms in the B_{15}^- cluster, which we believe are attributable to a similar 4σ delocalized system.

In short, the CMO analyses indicate that the B_{15}^+ cluster possesses three delocalized systems: 8π antiaromaticity for the π framework, 10σ aromaticity for the radial p_r σ framework, and 4σ antiaromaticity for the inner B_4 core, in addition to 11 localized 2c-2e σ bonds for the peripheral B_{11} ring. It is stressed that not a single 2c-2e σ bond can be identified from the CMOs for the B_4 core in the B_{15}^+ cluster. Boldyrev and coworkers[8] previously "assumed" four 2c-2e bonds for the B_4 core in B_{15}^-. We believe the Boldyrev model needs to be updated in light of our current analyses.[35] The bonding in the TS structure of B_{15}^+ (Fig. S2, ESI†) is nearly identical to that of the GM.

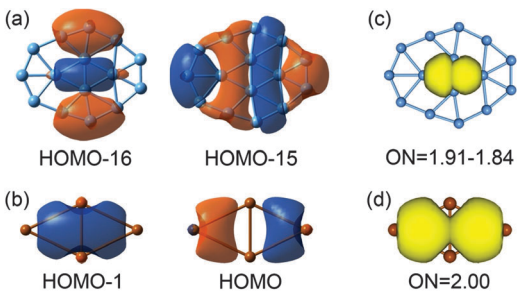

Fig. 4 Comparison of the two σ canonical molecular orbitals (CMOs) for (a) the rhombic B_4 core in B_{15}^+ and (b) Li_4 D_{2h} (^1A_g). Also compared are their corresponding three-center two-electron (3c-2e) σ bonds, (c) and (d), as revealed from AdNDP analyses. The occupation numbers (ONs) are shown.

3.3. ELF and AdNDP analyses: an approximate island view of a delocalized system

The above bonding picture of B_{15}^+ is fully supported by the ELF_σ and ELF_π patterns (Fig. 5(a)), which show 11 peripheral 2c-2e B–B σ bonds and hint for three-, four-, and five-center delocalized σ and π bonding in the cluster. The AdNDP data are also fully consistent with the bonding picture. The 11 peripheral B–B σ bonds (Fig. 5(b)) are readily recovered, as are the four "island" π bonds: two 3c-2e at the top and bottom, one 4c-2e at the left side, and one 5c-2e at the right. The global σ framework can be approximated to four σ islands that overlap spatially with the four π islands, as well as one complementary 12c-2e σ bond;[36,37] the ELF_σ density of the latter bond appears to be smeared out in the cluster (Fig. 5(a)), as anticipated. In Section 3.6 below, we shall offer further discussion on this AdNDP σ scheme (as well as an alternative AdNDP scheme). In addition, the inner B_4 core is held together by two 3c-2e σ bonds, akin to the σ antiaromatic Li_4 cluster (Fig. 4(c) and (d)).[38] Note that the ON values for two 3c-2e σ bonds in the inner B_4 core of B_{15}^+ are 1.84–1.91 (Fig. 4(c)), which are close to ideal. Thus the concept that the rhombic B_4 core is held together by four electrons is rather solid.

The island σ and π pictures (Fig. 5) suggest that the B_{15}^+ cluster is indeed composed of two triangular B_3, one rhombic B_4, and one trapezoid B_5, which fuse together to form an inner B_4 core, as well as four rhombic B_4 holes. These rhombic B_4 holes appear to be loosely bound with respect to the peripheral $B_3/B_4/B_5$ islands, as hinted by their larger peripheral B–B distances (Fig. 1(a)): B11–B10 (1.61 Å), B9–B8 (1.59 Å) *versus* B1–B11 (1.52 Å), B10–B9 (1.56 Å), and B7–B6 (1.52 Å). The island model also offers a simple way to partition the electrons in the system.[39]

While the three-center island bonds (two of them for σ; and two for π) have relatively low ONs of 1.62, these values are acceptable in the AdNDP analyses for electron-deficient boron clusters[12,21] because they represent an approximate 3c-2e island view for the truly delocalized frameworks with 8π and 10σ electrons, respectively (Fig. 3(a) and (c)). Note that even such 3c-2e islands catch as much as 80% of the essence with respect to a completely delocalized bond (ideal ON: 2.00). All other island bonds have ON values greater than 1.80, close to ideal. The island picture (Fig. 5(b)) is thus a sufficiently accurate presentation of the bonding, which turns out to be valuable for understanding the structural fluxionality and dynamic properties of B_{15}^+.

The 8π antiaromatic system in the B_{15}^+ cluster can be compared with those of its hydrocarbon analogues: cycloheptatrienyl radical (C_7H_7)[40] and cyclooctatetraene (C_8H_8). C_7H_7 is planar with C_{2v} symmetry, whose HOMO is only half-occupied, that is, the singly occupied molecular orbital (SOMO; Fig. 6). It is thus a 7π antiaromatic system. On the other hand, C_8H_8 is a true 8π system and undergoes substantial non-planar distortion to D_{2d} symmetry (Fig. 6(c)). The CMOs of the three species exhibit remarkable similarity (Fig. 6), suggesting that the B_{15}^+ cluster is an all-boron analogue of cycloheptatrienyl radical and cyclooctatetraene.

3.4. Structural and electronic evolution during the intramolecular rotation

Following the structural evolution of B_{15}^+ in the in-plane rotation process, we can easily map out the corresponding potential energy surface. Assume the cluster rotates clockwise, the process is illustrated in Fig. 7 with the aid of the AdNDP

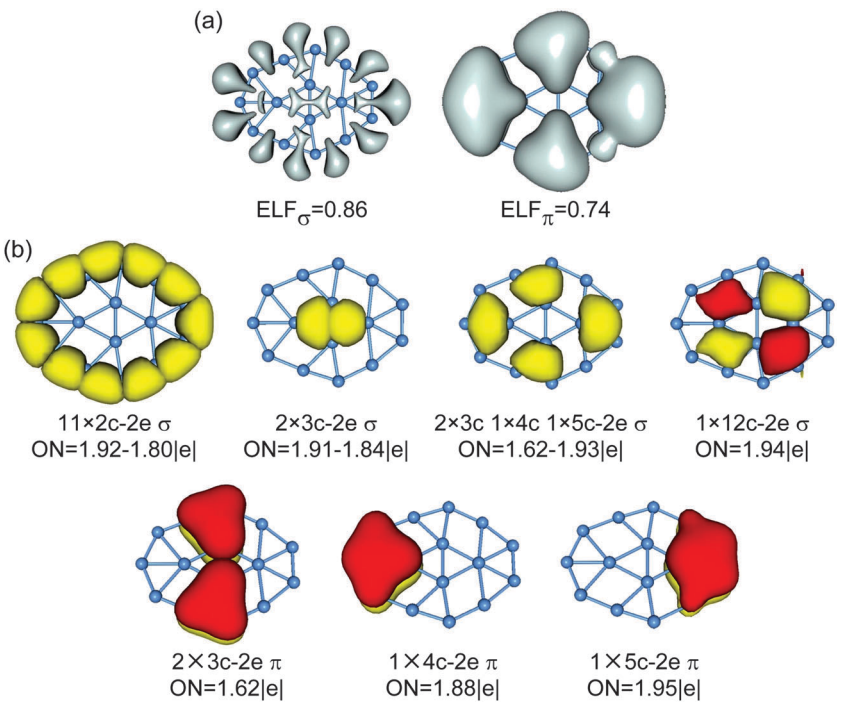

Fig. 5 Chemical bonding in the C_{2v} ($^1A_1$) global minimum of B_{15}^+. (a) Electron localization functions (ELFs). (b) Bonding elements as revealed from AdNDP analysis, along with the occupation numbers (ONs). AdNDP offers an alternative, "island" view of a delocalized system.

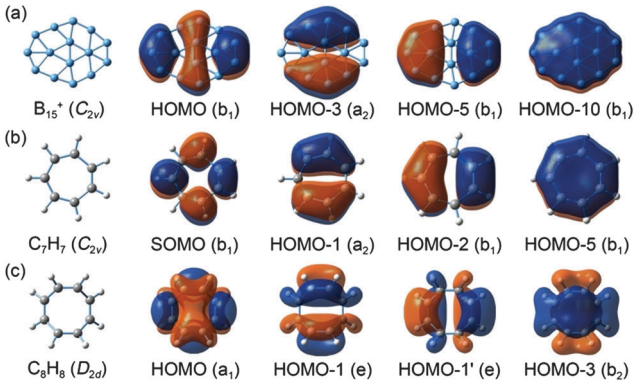

Fig. 6 Comparison of π canonical molecular orbitals (CMOs) of (a) C_{2v} B_{15}^+, (b) C_{2v} C_7H_7, and (c) D_{2d} C_8H_8. SOMO stands for the singly occupied molecular orbital.

data (Fig. 5(b); Fig. S3(b), ESI†). Only two structures are involved: the GM and the TS (Fig. 1).

At the initial GM_1 structure, the four σ islands are located on the rhombic B_4 at the left, two triangular B_3 at the top and bottom, and the trapezoid B_5 at the right (Fig. 7(a)). These are complemented by a 12c-2e σ bond that holds together the four $B_3/B_4/B_5$ islands (Fig. 7(b)). As the cluster rotates clockwise (that is, to the right side), the orientations of the σ islands shift slightly around the B_4 core, reaching the transition state TS_{1-2} (Fig. 7(a)). In this step, the island B_3 σ cloud at the bottom expands counter-clockwise to a B_4 island; whereas that of the B_5 σ bond at the right side shrinks slightly to a B_4 island, also in a counter-clockwise manner. For the remaining two islands, the electron cloud remains intact.

Passing the barrier, GM_2 is reached, which is equivalent to GM_1, except for a 180° in-plane rotation. From TS_{1-2} to GM_2, the electron cloud of the B_4 σ bond at the left side expands to a B_5 island and that of the B_4 σ bond at the bottom shrinks slightly to a B_3 island. The evolution from GM_2 to GM_3 *via* TS_{2-3} generally repeats the above process from GM_1 to GM_2 *via* TS_{1-2}, and the GM_3 structure recovers that of GM_1 both in structure and in orientation. However, every peripheral B atom in GM_3 shifts clockwise by one link with respect to that in GM_1; that is, the B_{15}^+ cluster moves by one link toward the right side.

In the whole process illustrated in Fig. 7(a), the orientation of the C_2 axis of GM/TS rotates four times, by 90° for each step. Interestingly, the direction of the flow of electron clouds persistently counters that of the structural rotation, which manages to maintain the island clouds at roughly the same orientation of the cluster despite the movement of the latter. Repeating the above process 11 times, the whole B_{15}^+ cluster will recover its exact initial structure and every peripheral B atom recovers its exact initial position. As a consequence, the whole cluster moves clockwise for one loop. The 12c-2e σ bond undergoes a similar evolution process (Fig. 7(b)), as are the four island π bonds (Fig. 8). Thus, the globally-delocalized 8π and 10σ bonds flow, shift, shrink, or expand continuously like liquid during the intramolecular rotation process. Each elemental step of these requires little extra energy, which

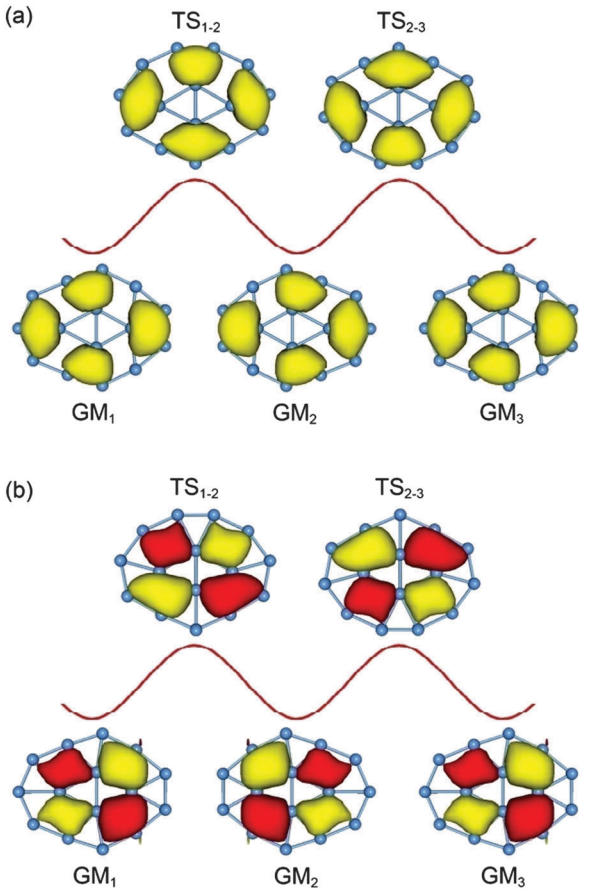

Fig. 7 Evolution processes of the structure and σ bonds during the in-plane rotation of the B_{15}^+ cluster. (a) The four σ bonds islanded on three/four/five centers. (b) The 12c-2e σ bond delocalized over the whole system. These five σ bonds are based on the AdNDP data. The cluster is assumed to rotate clockwise in the presentation.

underlies the structural fluxionality for the B_{15}^+ cluster as a nanoscale tank tread.

Actually, the nature of three-fold electron delocalization in B_{15}^+ (Fig. 3) suggests that there exists no 2c-2e bonds inside the peripheral B_{11} ring, despite the fact that as many as 16 and 18 such "bonds" are depicted for the GM and TS structures, respectively (Fig. 1). It should be stressed that none of those "bonds" is real. The fully delocalized electron clouds serve as an ideal "lubricant" for the rotation of B_{15}^+ as a tank tread.

3.5. Two soft modes as double engines for the nanoscale tank tread?

As described in Section 3.1, a soft in-plane rotational mode of 166.3 cm^{-1} for the GM structure of B_{15}^+, coupled with the rhombic "defective" holes, serves as an engine that drives the nanoscale tank tread forward. A rather similar mechanism underlies the intramolecular rotation of the prior B_{11}^- and B_{11} clusters,[21] except that B_{11}^- has a slightly smaller mode of 148.7 cm^{-1} and only one square hole. There are four rhombic, defective holes in B_{15}^+, as illustrated in Fig. 1(a), suggesting that it can be more difficult to drive the motion of such a tank tread. A closer examination of B_{15}^+ reveals that there exist actually two

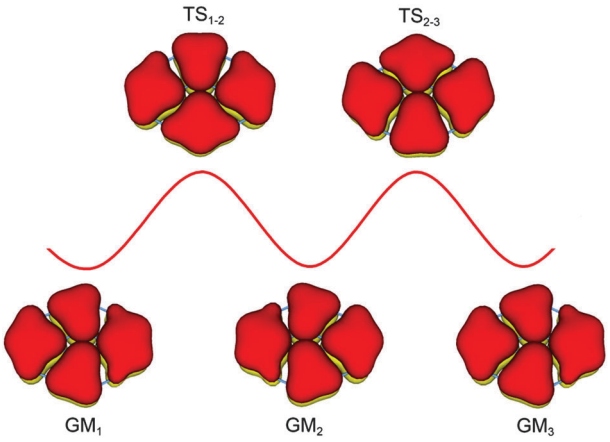

Fig. 8 The evolution process of π bonds during the peripheral ring rotation of the B_{15}^+ cluster. The pattern of π clouds is adopted from the AdNDP data.

vibrational modes for the intramolecular rotation (Fig. 2(a)), the greater being 258.3 cm^{-1}.

The 166.3 cm^{-1} mode uses the B12 atom as the axle and mainly involves the rhombus-to-square transformation of B11B10B15B12 and B2B3B13B12, driving by the up and down movement of atom B12 with marked displacements for the B12/B10/B3/B11/B2 atoms. However, for the right side of the cluster, the magnitude of structural changes is much smaller with discernible displacements only for the B8/B5 atoms. In other words, this mode does not seem to be capable of driving the rotation of the whole cluster, because the right-hand half of the cluster remains largely rigid.

The 258.3 cm^{-1} mode, on the other hand, exactly complements the above situation, which is based on the B14 atom as a second axle in the system. This mode exhibits notable movements of atoms B8 and B5, leading to the rhombus-to-square transformations of B8B9B15B14 and B5B4B13B14. In addition, it also drives the rhombus-to-square transformations of B11B10B15B12 and B2B3B13B12, but this should be considered as its secondary role. In order for the whole B_{15}^+ cluster to be structurally fluxional, we believe both of the 166.3 and 258.3 cm^{-1} modes are needed, which are complementary to each other and work in concert to drive the rotation of B_{15}^+ as a tank tread. The two modes may be dubbed "double engines", which are based on the B12 and B14 centers, respectively, as a unique double-axle system.

To further understand and confirm the "double engines" in the B_{15}^+ tank tread, it is instructive to compare it with another elongated boron cluster, B_{14}^-,[4] whose GM structure is well characterized as shown in Fig. S4, ESI.† It has only one soft mode of 283.1 cm^{-1}, which corresponds to the rotation around the B12 atom as an axle, similar to the B12 axle in B_{15}^+ (Fig. 2(a)). However, neither a second axle nor a second soft mode can be identified in B_{14}^- at the right side. Not surprisingly, the B_{14}^- anion cluster would not rotate as a tank tread even at the temperature of 900 K. Our preliminary PBE0 calculations indicate that the B_{14}^- cluster has a substantially higher rotational barrier, which is greater than 9 kcal mol^{-1}. The above comparisons suggest that the concept of double engines is critical in the B_{15}^+ cluster as a tank tread. The double-engine or double-axle concept may be applied to other nanosystems including boron clusters, but excluding B_{14}^- as discussed above. This fertile ground awaits forthcoming explorations. It is anticipated that, for elongated clusters with a further extended length than B_{15}^+, multiple modes are probably necessary in order to drive their structural fluxionality.

3.6. On an alternative AdNDP scheme for the σ framework

AdNDP is a user directed program.[29] An alternative AdNDP scheme for the 10σ system in Fig. 3(a) can be obtained as an "automatic" solution from the AdNDP program, which includes five 3c-2e σ bonds: B1B2B12, B11B1B12, B3B4B13, B10B15B9, and B6B7B14. Since a 3c-2e B6B7B14 σ bond is not much different from a 5c-2e B5B6B7B8B14 σ bond in the scheme described in Section 3.3, the two AdNDP σ schemes differ in the rhombic B1B2B12B11 island: the original scheme suggests one 4c-2e σ bond only (Fig. 5(b)), whereas the alternative scheme suggests two 3c-2e σ bonds (B1B2B12 and B11B1B12). We would like to reason that the alternative σ scheme is incorrect and counter-intuitive, which also offer in-depth understanding of the essence of bonding in the B_{15}^+ cluster.

First, the two 3c-2e σ bonds on the rhombic B1B2B12B11 island are inconsistent with the ELF_σ data (Fig. S5, ESI†). With increasing bifurcation values, the island ELF_σ density in the B1B2B12B11 rhombus is more clearly shown to be maximized on the B1B12 diagonal (rather than to shrink and to be separated as two three-center islands), indicating a single 4c-2e σ bond here. There is no evidence for two 3c-2e σ bonds within this region according to the ELF_σ data.

Second, the in-plane rotation from GM_1 to GM_2 *via* TS_{1-2} (Fig. 7(a)) should be a continuous process both physically and chemically, even if the cluster were not fluxional. However, following the alternative AdNDP σ scheme, there are two 3c-2e σ bonds on the left side in GM_1 (and one on the right side), and after a slight rotation of the peripheral ring by half a link there are only one 3c-2e σ bond on the left side in GM_2 (and two on the right side). This evolution suggests that, upon rotation by half a link, there has to be an "*annihilation*" of one 3c-2e σ bond on the left side and a "*creation*" of one 3c-2e σ bond on the right side; or one 3c-2e σ island bond has to "*hop*" from the left side to the right side upon slight rotation of the peripheral ring. Similarly, for the next half cycle from GM_2 to GM_3, there has to be a "creation" of one 3c-2e σ bond on the left side and an "annihilation" of one 3c-2e σ bond on the right side. The above "annihilation/creation" processes are counter-intuitive for a molecule, both in physics and in chemistry.

Third, in the original AdNDP scheme (Section 3.3), every single electron for every B center can be counted simply.[39] For the alternative AdNDP scheme, however, one has to conclude that the inner B_4 core is bound *via* two electrons from B14, one electron from B15, one electron from B13, and no electron from B12. Specifically, the B1B2B12B11 rhombus has 12 valence electrons, of which six are used for the peripheral 2c-2e B3B2,

B2B1, B1B11, and B11B10 σ bonds and two are for the island π bond. If two 3c-2e σ bonds (four electrons) were indeed present in the B1B2B12B11 rhombus, all 12 valence electrons are exhausted and there is no electron from the rhombus to facilitate bonding within the inner B_4 core. For such a situation, substantial electron transfers need to take place from B15/B13 to B12, as well as from B14 to B15/B13, in order to make the two 3c-2e σ bonds in the B_4 core. In other words, B14 should be positively charged and B12 should be negative. Unfortunately, the NBO charges indicate that the B12 center is practically neutral (+0.05 $|e|$) and the B15/B13/B14 centers are slightly negative (about −0.25 $|e|$). Thus the NBO charges also suggest that the alternative AdNDP σ scheme is invalid.

4. Conclusions

In conclusion, we have computationally investigated the molecular dynamic properties and chemical bonding of a planar, elongated B_{15}^+ cation cluster, using electronic structure calculations, Born–Oppenheimer molecular dynamics simulations, canonical molecular orbitals, electron localization functions, and adaptive natural density partitioning analyses. The elongated B_{15}^+ cluster is shown to be structurally fluxional at 500 K and beyond, whose peripheral B_{11} ring rotates almost freely around a rhombic B_4 core, akin to a moving tank tread at the nanoscale. The in-plane rotational energy barrier is 1.37 and 1.66 kcal mol^{-1} at the PBE0 and single-point CCSD(T) levels, respectively. Two soft vibrational modes, dubbed ''double engines'', are revealed around two rotational axles, which are complementary to each other and work in concert to drive the intramolecular rotation of the B_{15}^+ cluster. A bonding model is proposed for B_{15}^+, which features three-fold electron delocalization: 8π antiaromaticity for the global π framework, 10σ aromaticity for the global radial p_r σ framework, and 4σ antiaromaticity for the inner B_4 core. The model helps elucidate the intriguing molecular dynamics of the cluster.

Acknowledgements

This work was supported by the National Natural Science Foundation of China (21573138, 21243004), the Innovation Program of Postgraduate Education of Shanxi Province (2016BY011), and the State Key Laboratory of Quantum Optics and Quantum Optics Devices (KF201402).

References

1 C. Joachim and G. Rapenne, *ACS Nano*, 2013, **7**, 11.
2 Y. Shirai, J. F. Morin, T. Sasaki, J. M. Guerrero and J. M. Tour, *Chem. Soc. Rev.*, 2006, **35**, 1043.
3 H. J. Zhai, A. N. Alexandrova, K. A. Birch, A. I. Boldyrev and L. S. Wang, *Angew. Chem., Int. Ed.*, 2003, **42**, 6004.
4 H. J. Zhai, B. Kiran, J. Li and L. S. Wang, *Nat. Mater.*, 2003, **2**, 827.
5 A. N. Alexandrova, A. I. Boldyrev, H. J. Zhai and L. S. Wang, *Coord. Chem. Rev.*, 2006, **250**, 2811.
6 A. P. Sergeeva, I. A. Popov, Z. A. Piazza, W. L. Li, C. Romanescu, L. S. Wang and A. I. Boldyrev, *Acc. Chem. Res.*, 2014, **47**, 1349.
7 I. A. Popov and A. I. Boldyrev, Classical and Multicenter Bonding in Boron: Two Faces of Boron, in *Boron. The Fifth Element*, ed. D. Hnyk and M. L. McKee, Springer International Publishing, Switzerland, 2015, pp. 1–16.
8 D. Yu. Zubarev and A. I. Boldyrev, *J. Comput. Chem.*, 2007, **28**, 251.
9 W. Huang, A. P. Sergeeva, H. J. Zhai, B. B. Averkiev, L. S. Wang and A. I. Boldyrev, *Nat. Chem.*, 2010, **2**, 202.
10 T. B. Tai, R. W. A. Havenith, J. L. Teunissen, A. R. Dok, S. D. Hallaert, M. T. Nguyen and A. Ceulemans, *Inorg. Chem.*, 2013, **52**, 10595.
11 A. P. Sergeeva, Z. A. Piazza, C. Romanescu, W. L. Li, A. I. Boldyrev and L. S. Wang, *J. Am. Chem. Soc.*, 2012, **134**, 18065.
12 W. L. Li, Y. F. Zhao, H. S. Hu, J. Li and L. S. Wang, *Angew. Chem., Int. Ed.*, 2014, **53**, 5540.
13 W. L. Li, Q. Chen, W. J. Tian, H. Bai, Y. F. Zhao, H. S. Hu, J. Li, H. J. Zhai, S. D. Li and L. S. Wang, *J. Am. Chem. Soc.*, 2014, **136**, 12257.
14 Z. A. Piazza, H. S. Hu, W. L. Li, Y. F. Zhao, J. Li and L. S. Wang, *Nat. Commun.*, 2014, **5**, 3113.
15 H. J. Zhai, Y. F. Zhao, W. L. Li, Q. Chen, H. Bai, H. S. Hu, Z. A. Piazza, W. J. Tian, H. G. Lu, Y. B. Wu, Y. W. Mu, G. F. Wei, Z. P. Liu, J. Li, S. D. Li and L. S. Wang, *Nat. Chem.*, 2014, **6**, 727.
16 B. Kiran, S. Bulusu, H. J. Zhai, S. Yoo, X. C. Zeng and L. S. Wang, *Proc. Natl. Acad. Sci. U. S. A.*, 2005, **102**, 961.
17 E. Oger, N. R. M. Crawford, R. Kelting, P. Weis, M. M. Kappes and R. Ahlrichs, *Angew. Chem., Int. Ed.*, 2007, **46**, 8503.
18 J. O. C. Jiménez-Halla, R. Islas, T. Heine and G. Merino, *Angew. Chem., Int. Ed.*, 2010, **49**, 5668.
19 G. Martínez-Guajardo, A. P. Sergeeva, A. I. Boldyrev, T. Heine, J. M. Ugalde and G. Merino, *Chem. Commun.*, 2011, **47**, 6242.
20 D. Moreno, S. Pan, L. L. Zeonjuk, R. Islas, E. Osorio, G. Martínez-Guajardo, P. K. Chattaraj, T. Heine and G. Merino, *Chem. Commun.*, 2014, **50**, 8140.
21 Y. J. Wang, X. Y. Zhao, Q. Chen, H. J. Zhai and S. D. Li, *Nanoscale*, 2015, **7**, 16054.
22 S. Erhardt, G. Frenking, Z. F. Chen and P. R. Schleyer, *Angew. Chem., Int. Ed.*, 2005, **44**, 1078.
23 C. Adamo and V. Barone, *J. Chem. Phys.*, 1999, **110**, 6158.
24 R. Krishnan, J. S. Binkley, R. Seeger and J. A. Pople, *J. Chem. Phys.*, 1980, **72**, 650.
25 M. J. Frisch, *et al.*, *Gaussian 09, revision D.01*, Gaussian Inc., Wallingford, Connecticut, 2009.
26 G. D. Purvis and R. J. Bartlett, *J. Chem. Phys.*, 1982, **76**, 1910.
27 J. VandeVondele, M. Krack, F. Mohamed, M. Parrinello, T. Chassaing and J. Hutter, *Comput. Phys. Commun.*, 2005, **167**, 103.

28 B. Silvi and A. Savin, *Nature*, 1994, **371**, 683.
29 D. Yu. Zubarev and A. I. Boldyrev, *Phys. Chem. Chem. Phys.*, 2008, **10**, 5207.
30 U. Varetto, *Molekel 5.4.0.8*, Swiss National Supercomputing Center, Manno, Switzerland, 2009.
31 H. J. Zhai, Q. Chen, H. Bai, H. G. Lu, W. L. Li, S. D. Li and L. S. Wang, *J. Chem. Phys.*, 2013, **139**, 174301.
32 H. J. Zhai, Q. Chen, H. Bai, S. D. Li and L. S. Wang, *Acc. Chem. Res.*, 2014, **47**, 2435.
33 J. M. Mercero, A. I. Boldyrev, G. Merino and J. M. Ugalde, *Chem. Soc. Rev.*, 2015, **44**, 6519.
34 A. N. Alexandrova and A. I. Boldyrev, *J. Phys. Chem. A*, 2003, **107**, 554.
35 Our analyses show that the B_{15}^- and B_{15}^+ clusters differ by one extra CMO in the former, which is the p_r σ HOMO.[8] All other CMOs show one-to-one correspondence with each other for the two species. Thus, B_{15}^- should also possess three-fold electron delocalization: 8π antiaromaticity for the global π framework, 12σ antiaromaticity for the global radial p_r σ framework, and 4σ antiaromaticity for the inner B_4 core. To our knowledge, three-fold antiaromaticity in a molecule is quite unusual in chemistry. This may be considered as an update for the Boldyrev bonding model[8] of B_{15}^-.
36 The island AdNDP localization for the five σ CMOs in Fig. 3(a) is readily rationalized as follows. Such localization cannot be anticipated to be perfect because this is a 10σ aromatic system, whose five CMOs are intrinsically, fully delocalized. To achieve an approximate island view, one is allowed to adopt a "hybrid" scheme, that is, four 3c-2e/4c-2e/5c-2e island σ bonds plus one "residual" 12c-2e σ bond as shown in Fig. 5(b). A completely localized island picture is simply not feasible or reasonable due to geometric reasons for this specific cluster. Note that for an aromatic 10σ system, an AdNDP scheme with a higher degree of overall localization does not necessarily mean a more reasonable, chemically-intuitive scheme.
37 The hybrid AdNDP σ scheme shown in Fig. 5(b) is understandable considering that the five σ *versus* four π CMOs shown in Fig. 3(a) and (c) are closely parallel to each other in terms of spatial distribution, except for an extra HOMO−4 for the σ framework. Thus, HOMO−1, HOMO−2, HOMO−9, and HOMO−6 are collectively localized as four island σ bonds in AdNDP, just as HOMO, HOMO−5, HOMO−3, and HOMO−10 are islanded as four π bonds on the same set of islands (four in total). This leaves HOMO−4 for a "residual", more delocalized σ bond, as also revealed in AdNDP as a 12c-2e σ bond (Fig. 5(b)). It is stressed that this 12c-2e σ bond is also C_{2v} symmetric in terms of the spatial distribution of the electron cloud (albeit the upper and lower portions differ in sign: "+" *versus* "−"), which will not break the C_{2v} symmetry of the cluster.
38 The notion that antiaromaticity can be alternatively described as island aromaticity is well established.[5] Thus 4π antiaromatic cyclobutadiene (C_4H_4) has alternating single and double bonds. Similarly, the 4σ delocalized electrons for a rhombic B_4 or Li_4 cluster[34] can be approximated to two 3c-2e σ islands (Fig. 4(c) and (d)). This AdNDP pattern is routine, in line with 4σ antiaromaticity.
39 This discussion is within the island approximation (Fig. 5(b)). Briefly, the two B_3, one B_4, and one B_5 structural units in the B_{15}^+ cluster have 9, 12, and 15 electrons, respectively, of which 2, 4, and 6 are used for the peripheral B–B σ bonds. Next, 2 electrons for each unit are responsible for the "fusion" of the fragments (that is, to form part of the peripheral B–B σ framework) and 4 electrons for each unit are used for island π and σ bonds. Thus, only 1, 2, and 3 electrons remain for the B_3, B_4, and B_5 units, respectively. The B_5 unit appears to be relatively electron-rich and should contribute to the extra positive charge in the cation, and each unit offers one electron to the σ bonding in the inner B_4 core. Lastly, the B_4 and B_5 units each have one electron, leading to the formation of the global 12c-2e σ bond.
40 A. D. Allen and T. T. Tidwell, *Chem. Rev.*, 2001, **101**, 1333.

